Effect of crossflow on trapping depths of particle plumes: laboratory experiments and application to the PLUMEX field experiment

As Published: https://doi.org/10.1007/s10652-021-09795-5

Publisher: Springer Netherlands

Persistent URL: https://hdl.handle.net/1721.1/136921

Version: Author's final manuscript: final author's manuscript post peer review, without publisher's formatting or copy editing

Effect of crossflow on trapping depths of particle plumes: laboratory experiments and application to the PLUMEX field experiment

Cite this article as: Dayang Wang, E. Eric Adams, Carlos Munoz-Royo, Thomas Peacock and Matthew H. Alford, Effect of crossflow on trapping depths of particle plumes: laboratory experiments and application to the PLUMEX field experiment, Environmental Fluid Mechanics https://doi.org/10.1007/s10652-021-09795-5

Effect of Crossflow on Trapping Depths of Particle Plumes: Laboratory Experiments and Application to the PLUMEX Field Experiment

Dayang Wang[1, †], E. Eric Adams[2], Carlos Munoz-Royo[3], Thomas Peacock[3], Matthew H. Alford[4]

[1] Exponent, Massachusetts, USA.

[2] Department of Civil and Environmental Engineering, Massachusetts Institute of Technology, Massachusetts, USA.

[3] Department of Mechanical Engineering, Massachusetts Institute of Technology, Massachusetts, USA.

[4] Scripps Institution of Oceanography, University of California, California, USA.

Corresponding author: Dayang Wang (wangd04@gmail.com)

† Corresponding author's current address is Exponent, 1 Mill and Main Place, Suite 150, Maynard, Massachusetts 01754, USA.

Keywords:

Particle plumes, intrusion, multi-phase flow, PLUMEX field experiment, deep-sea mining

Key points:

- Laboratory measurements of trap depth are presented for particle plumes in stratification under conditions of weak to strong crossflow and weak to moderate particle settling velocity.
- Trap depths decline exponentially with crossflow but show little sensitivity to settling velocity in the range studied.
- The empirical correlation is validated by the PLUMEX field experiment involving simulated disposal of deep-sea mining wastes.

1. Introduction

The fate and transport of multi-phase plumes in the ocean environment, such as an oil plume following an oil spill and a sediment plume during the disposal of deep-sea mining residuals, are affected by crossflow. Socolofsky & Adams, (2002) categorize the plume flow into two regimes: stratification- or crossflow-dominated regimes. The main difference between these two regimes is the dominant forcing responsible for causing detrainment (separation) of the continuous phase (the entrained ambient seawater) from the dispersed phase (e.g., the sediments in a sediment plume; Akar & Jirka, 1994, 1995; Wang & Adams, 2016; Dissanayake et al., 2018). The detrained fluid becomes trapped at a level of neutral buoyancy and spreads radially into the surrounding ambient as an intrusion. The vertical distance between the discharge and the intrusion is termed trap depth. When a plume is stratification-dominated, the continuous phase undergoes detrainment when it reaches the neutrally buoyant level. The resulting trapping depth depends on the ambient stratification (Socolofsky & Adams, 2002). Conversely, in the crossflow-dominated regime, fluid detrainment takes place due to strong crossflow, which forcibly advects the fluid in the downstream direction, thereby separating it from the plume before it reaches the neutrally buoyancy level. There exists a transitional current speed $U_{a,trans}$, distinguishing crossflow from stratification dominance (Socolofsky & Adams, 2002; Wang & Adams, 2016; Dissanayake et al., 2018). We note that while the mechanisms causing detrainment of rising droplet and sinking particle plumes are similar, we refer simply to particle plumes.

To define $U_{a,trans}$, Wang & Adams (2016) first identify the independent parameters used for characterizing a multi-phase plume: the total initial kinematic buoyancy flux $B=g'Q_o$ of the plume where g' is the reduced gravity and Q_o is the total initial flow rate of oil, the stratification frequency $N = \sqrt{g\partial\rho/\rho\partial z}$ of the ambient water where ρ and z are the ambient water density and water depth respectively, the ambient current velocity U_a and the individual particle settling (slip) velocity U_s, which correlates directly to particle size. The smaller the particle size, the slower the particle settling (slip) velocity. Using B and N as repeating variables, characteristic length and velocity scales can be defined as follows (Fischer, et al., 1979; Morton, Taylor, & Turner, 1956):

$$L_c = \left(\frac{B}{N^3}\right)^{1/4} \quad (1)$$

$$U_c = (BN)^{1/4} \quad (2)$$

$U_{a,trans}$ can be expressed as the relative strengths of ambient and particle slip velocities; based on a fit to data in Socolofsky & Adams (2002),

$$\frac{U_{a,trans}}{U_c} \cong \left(\frac{U_c}{U_s}\right)^2 \quad (3)$$

When U_a is bigger than $U_{a,trans}$, the flow transitions from stratification-dominated to crossflow-dominated. The intrusion layers in the crossflow-dominated regime have been studied by several authors (Akar & Jirka, 1994; Socolofsky & Adams, 2002).

At U_a = 0, the plume is stratification-dominated. The intrusion layers in this regime have been studied by several authors, e.g., Asaeda & Imberger (1993); Chan et al. (2014) ; Johansen et al. (2003); Lemckert & Imberger, 1993a, 1993b; McDougall, 1978; Mingotti & Woods, 2019; and Socolofsky & Adams, 2005. Notably, based on their laboratory experiments, Socolofsky & Adams (2005) calibrated the following empirical relationship for the trap depth h_T under stagnant conditions in terms of characteristic length L_c and a non-dimensional slip velocity, $\frac{U_s}{U_c}$:

$$\frac{h_T}{L_c} = \emptyset_1\left[\frac{U_s}{U_C}\right]. \quad (4)$$

In this study, we consider an updated form of their original relation calibrated on revised datasets (see Section 3).

The transition between regimes does not happen abruptly and the flow for $U_a \approx U_{a,trans}$ remains largely unexplored (Dissanayake et al., 2018). Our study investigates the influence of crossflow velocity on plume trap depth in stratification with a range of crossflows —conditions typical of those expected during the deep-sea mining waste disposal. We develop an empirical relationship for normalized h_T which spans the range from weak to strong crossflows.

Two sets of experiments, each set simulating a crossflow in different ways, were conducted (see next section). Inert glass particles used to simulate sediments were released continuously into stratified water in a laboratory tank. Based on the experimental results, an analytical relation was developed for predicting the trap depth of a plume by considering both the influence of crossflow and stratification. The model was applied to predict a plume generated in a field experiment where

actual deep-sea sediments were used to simulate the fate of residuals released at midwater depths as a result of deep-sea nodule mining. Additionally, a numerical model was applied for comparison with the laboratory and field measurements, as well as with the analytical results.

2. Experiment set-ups

2.1. Experiment 1: Long tank with towed discharge

The first set of experiments took place in a towing tank by towing a discharge source at constant velocity in an acrylic flume with dimensions 5 m (L) x 1.2 m (W) x 0.6 m (H) (Figure 1). Ambient water was linearly stratified with salt using the two-tank method as described by Hill (2002). The simulated stratification frequency, N, varied with the amount of salt used for stratification in the experiments. When the tank was being filled in preparation for an experiment, a buoyant plate was placed between the water surface and the filling hose to redirect the impinging water flow and minimize vertical mixing. The sponge layer overlaying the plate surface dampened momentum, further minimizing mixing, thus maintaining stratification. Spherical glass beads with specific gravity of 2.5 were released as a dense slurry at a constant rate from a carboy mounted on a carriage at the top of the tank while the towing carriage moved at constant speeds. To ensure steady state condition, beads were not released during the initial acceleration or final deceleration of the towing carriage, but only while the carriage was moving at constant speed. A second carboy contained brine with a density matching that of the ambient water at the level of discharge. The brine was released together with the beads to make the flow more uniform without adding extra buoyancy or significant momentum or volume flow. Entrained fluid with Rhodamine dye, and particles in the plume and the intrusion layer were observed visually during the experiment and the dye was measured in-situ with a fluorometer following each experiment. Typically, 3-4 dye profiles were collected at distances of 1-3 m “downstream” from the point of discharge approximately 2-3 minutes after cessation of the experiment. Signal processing, as described in Supplementary Information Section 2.1, was performed on the measured profiles to smoothen the curves and informed the trap depth using the profile’s first moment. The trap depths for repeat profiles in a given experiment were then arithmetically averaged.

The relative motion between the towed discharge and bottom sled and the stationary water in the tank created an effect equivalent to that of pushing a stratified crossflow, with the obvious

advantage that a uniform current can be simulated. A potential artifact was the lack of ambient turbulence. However, Wright (1984) compared results with a towed source in a stationary ambient fluid, with results for a stationary source in an actual crossflow. The study identified little difference in plume behavior, suggesting that ambient turbulence plays a secondary role in influencing the plume behavior. Additional information concerning the experimental set up can be found in Wang & Adams (2016).

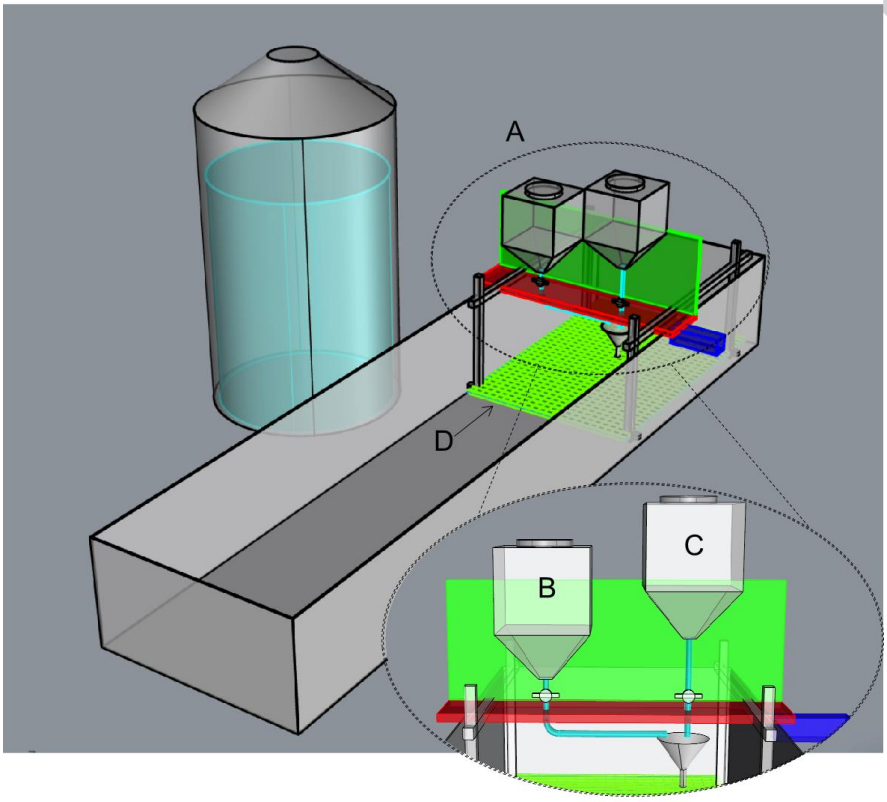

Figure 1. Schematic of experimental apparatus. (A) the towed discharge, (B) carboy containing glass beads, (C) carboy containing brine, (D) the bottom sled. The discharge point (funnel orifice) is 3 to 5 cm below the water surface and the discharge orifice diameter was 0.9 cm [figure adapted from Wang & Adams (2016)].

Our experiments explored the effect of varying U_s and U_a while keeping the values of B and N approximately constant. Potentially, source flow rate and momentum may play a role near the source, but these factors were of secondary importance in our experiments. The assumption that B dominates over Q_o and kinematic discharge momentum M can be justified by keeping the momentum (N_m) and volume (N_q) numbers, defined by Equations (5) and (6) (Fischer, et al., 1979; Morton et al., 1956; Chow, 2004) smaller than about one.

$$N_m = \frac{MN}{B} \quad (5)$$

$$N_q = \frac{Q_o^{4/3} N^{5/3}}{B} \quad (6)$$

Eight sizes of glass beads (A to AH) with median diameters ranging from 64 to 720 um were used (Table 1). The settling (slip) velocity was determined as a function of diameter and buoyancy from Dietrich (1982). A complete table of experimental conditions is presented in Table 2.

Table 1. Ballotini Impact Beads types and sizes as specified by Potters Industries LLC.

Particle Name	Range of Diameters (um)	Median Diameter D (um)	Particle density ρ (kg/m^3)	Range of Slip Velocities (cm/s)	Median Slip Velocity U_s (cm/s)
A	600-850	720	2450	8.3-12.1	10.2
B	425-600	510	2450	5.5-8.3	7.0
C	250-425	320	2450	2.7-5.5	4.1
D	212-300	250	2450	2.2-3.5	2.9
AD	106-212	150	2450	0.7-2.2	1.4
AE	90-150	120	2450	0.6-1.3	0.9
AG	53-125	81	2450	0.2-1.0	0.6
AH	45-90	64	2450	0.2-0.6	0.3

As indicated above, the depth from the water surface at which the descending particle plumes trapped and intruded was observed for the varying U_a using fluorescence measurements. Preliminary laboratory experiments in the towing tank suggested that crossflow played a significant role in affecting h_T. [see Figure 5 in Wang & Adams (2016)]. For two plumes in mild (stratification-dominated flow) and strong (current-dominated flow) crossflow velocities, the corresponding intrusion formation was notably different: the plumes under mild crossflow

condition showed distinctively shallower h_T compared to previous experiments in stagnant ambient, and the experiment that fell in the current-dominated regime showed even shallower h_T.

The towing tank was limited to a depth of 0.6m, which means that for some parameter combinations, the plume might have hit the bottom of the tank. Therefore, we conducted additional experiments using a taller tank, but its length did not permit the discharge to be towed as a way to create crossflow; thus, another way of simulating the crossflow was used in the tall tank experiments.

2.2. Experiment 2: Tall tank with rotating discharge

The second set of experiments was carried out in a glass tank with dimensions 2.5m (W) x 1.1m (L) x 2.2m (H) (Figure 2). As in the first experiments, stratification was created using salt following the two-tank method described by Hill (2002) and maintained with a buoyant plate whiling filling the tank. The simulated stratification frequency, N, varied with the amount of salt used for stratification in the experiments.

The container containing the discharge was attached to the end of a rotating shaft driven by a motor and set in a circular motion at the beginning of the experiment (Figure 2). The distance between the point of discharge and the rotating shaft was about 30cm. Glass particles with Rhodamine dye began to discharge by unplugging the rubber plugs at the bottom of the container. The release continued from the revolving container until the container was empty. The relative motion between the discharge and stagnant water created an equivalent effect of having a crossflow. The simulated crossflow velocity was adjusted by changing the angular velocity of rotation. The adjustable discharge apparatus allowed different discharge flow rates, thus the buoyancy flux B, to be achieved for each experiment (Supplementary Information, Section 1.1).

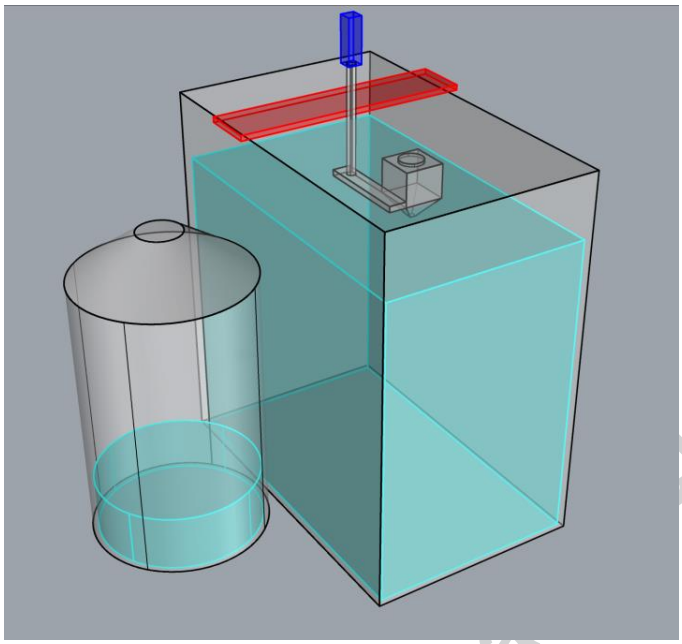

Figure 2. Schematic of the experimental setup: circular mixing tank for stratification, rectangular experimental tank with linearly stratified water and surface discharge container attached to a vertical rotating rod driven by a motor (blue box on top of the rod). The discharge apparatus is affixed to a horizonal plank (red) across the top of the tank. The discharge point (funnel) is 3 to 5 cm below the water surface (for details see Supplementary Information, Section 1).

Three bead sizes (B, C and AD) with properties outlined in Table 1 were used (only one size used in each set of the experiment) for simulating different slip velocities, U_s.

Dye profiles were measured with a fluorometer several minutes after cessation of discharge at a distance of ~1 m from the point of discharge. As with the earlier experiments, typically 3-4 dye profiles were collected. As with the first set of experiments, signal processing, as described in Supplementary Information Section 2.1, was performed on the measured profiles to smoothen the curves and informed the trap depths using the profile's first moment. The trap depths for repeat profiles in a given experiment were then arithmetically averaged.

The experimental conditions for both set of experiments, as well as the measured trap depth, are summarized in Table 2. There are four experiments for which U_a is bigger than $U_{a,\ trans}$, an indication that they are crossflow-dominated.

Particle plumes can differ from single phase plumes in an important respect discussed by Mingottti and Woods (2019). The particles provide the source of (negative) buoyancy and, the slower settling ones may enter and remain for some time in the intrusion (Chan et al., 2014). However,

ultimately, they settle out of the intrusion. The resulting loss of (negative) buoyancy causes the plume to "rebound". The depth of settling can be approximated as $U_s T_s$, where T_s is the elapsed time since the particles were released. For experiments in both the linear and rotating tanks, the elapsed time was sufficient to allow all of the particles to have settled out of the intrusion.

Table 2. Summary of experimental conditions

Exp_ID	Particle median diameter (μm)	U_a (m/s)	B (m^4/s^3 x 10^{-4})	N (s^{-1})	U_s (m/s x 10^{-3})	U_c (m/s)	U_s / U_c	$U_{a,\ trans}$ (m/s)	h_T (m)
LIN26	64	0.02	0.02	0.70	3.40	0.03	0.10	3.00	0.08
LIN27	81	0.02	0.04	0.72	5.50	0.04	0.13	2.37	0.13
LIN28	120	0.02	0.09	0.69	9.10	0.05	0.18	1.54	0.16
LIN30	150	0.02	0.14	0.77	28.50	0.06	0.50	0.24	0.16
LIN31	150	0.02	0.16	0.73	14.20	0.06	0.24	1.04	0.16
LIN32	250	0.02	0.15	0.75	28.50	0.06	0.49	0.25	0.18
LIN33	320	0.02	0.14	0.78	41.40	0.06	0.73	0.11	0.16
LIN34	320	0.02	0.16	0.77	41.40	0.06	0.70	0.12	0.15
LIN35	510	0.02	0.11	0.88	69.60	0.06	1.25	0.04	0.16
LIN36	720	0.02	0.10	0.87	101.60	0.05	1.89	0.01	0.13
LIN37	720	0.10	0.10	0.90	101.60	0.05	1.87	0.01	0.04
LIN38	150	0.02	0.16	0.74	14.20	0.06	0.24	1.04	0.16
LIN39	320	0.02	0.15	0.70	41.40	0.06	0.73	0.11	0.17
LIN40	320	0.05	0.15	0.71	41.40	0.06	0.73	0.11	0.13
LIN41	64	0.05	0.14	0.46	3.40	0.05	0.07	10.20	0.21
LIN42	81	0.05	0.22	0.48	5.50	0.06	0.10	6.00	0.20

ROT6.11.17C	320	0.04	0.09	0.07	41.40	0.03	1.46	0.01	0.38
ROT16.11.17C	320	0.08	0.54	0.15	41.40	0.05	0.78	0.08	0.45
ROT4.12.17AD	150	0.08	0.55	0.15	14.20	0.05	0.26	0.74	0.46
ROT1.12.17AD	150	0.06	0.55	0.16	14.20	0.05	0.26	0.74	0.56
ROT8.12.17AD	150	0.10	0.55	0.18	14.20	0.06	0.25	0.96	0.30
ROT15.11.17C	320	0.06	0.54	0.15	41.40	0.05	0.78	0.08	0.45
ROT2.10.17B	510	0.00	0.09	0.18	69.60	0.04	1.96	0.01	0.61
ROT5.10.17AD	150	0.00	0.09	0.16	14.20	0.04	0.40	0.25	0.59
ROT13.12.17C	320	0.00	0.27	0.15	41.40	0.05	0.92	0.06	0.76
ROT19.12.17B	510	0.00	0.27	0.17	69.60	0.05	1.50	0.02	0.79
ROT31.7.18B1	510	0.00	0.27	0.20	69.60	0.05	1.45	0.02	0.69
ROT3.8.18B3	510	0.00	0.27	0.19	69.60	0.05	1.46	0.02	0.73
ROT8.8.18C5	320	0.00	0.45	0.21	41.40	0.06	0.74	0.11	0.73
ROT17.8.18AD1	150	0.00	0.09	0.19	14.20	0.04	0.39	0.26	0.58
ROT20.8.18AD1	150	0.00	0.09	0.20	14.20	0.04	0.38	0.28	0.60
ROT23.8.18AD1	150	0.00	0.09	0.16	14.20	0.03	0.41	0.18	0.36
ROT24.8.18AD1	150	0.00	0.09	0.19	14.20	0.04	0.39	0.26	0.60
ROT25.8.18AD1	150	0.00	0.09	0.17	14.20	0.04	0.40	0.25	0.61

3. Analytical model for trap depth

In both sets of experiments, we observed a reduction in trap depth with increase in crossflow (Figure 4). Therefore, the effect of crossflow on the trap depth, by way of crossflow-induced (or "forced") entrainment, should be considered in modeling both crossflow- and stratification-dominated plumes. An analytical expression for $\frac{h_T}{L_c}$, the normalized depth of neutral buoyancy (or

trap depth) is assumed for a plume generated from a continuous buoyancy source in a stratified environment:

$$\frac{h_T}{L_c} = \emptyset_1\left[\frac{U_s}{U_C}\right]\emptyset_2\left[\frac{U_a}{U_C}\right], \qquad (7)$$

where $\emptyset_1$ and $\emptyset_2$ are dimensionless groups that are functions of the normalized particle settling velocity, $\frac{U_s}{U_c}$, and the normalized crossflow velocity, $\frac{U_a}{U_c}$, respectively. The functional form of $\emptyset_1$ is modified from Socolofsky & Adams, (2005) as follows:

$$\emptyset_1\left[\frac{U_s}{U_c}\right] = 2.8 - 0.066\frac{U_s}{U_c}, \qquad (8)$$

where the constant 2.8 corresponds to the value approached by $\frac{h_T}{L_c}$ for the limiting case of a single-phase plume (Morton et al., 1956), and the second term suggests that $\frac{h_T}{L_c}$ is weakly dependent on $\frac{U_s}{U_c}$. We re-analyzed the data in Figure 5 in Socolofsky & Adams (2005), and the results are presented in Figure 3**Error! Reference source not found.Error! Reference source not found.Error! Reference source not found.Error! Reference source not found.Error! Reference source not found.Error! Reference source not found.**, which shows mild dependence of h_T on U_N. The best-fit curve plotted in the figure is shown in equation (8), which approaches the result for the single-phase case, $h_T / L_c = 2.8$, for $U_N = 0$ (Morton, Taylor, & Turner, 1956).

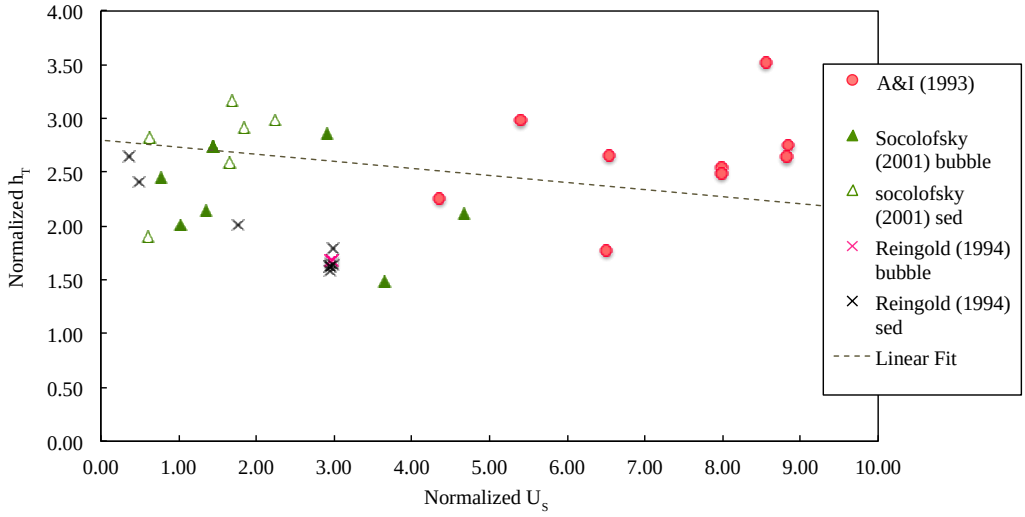

Figure 3. Correlation of trap depth (or height) to normalized U_s (U_s/U_c). The plot serves as an update on Figure 5 in Socolofsky & Adams (2005).

To find the expression for f_2, we first plot the laboratory observed trap depth, in the rearranged form $\frac{h_T}{L_c \phi_1}$ against normalized crossflow velocity $\frac{U_a}{U_c}$, as shown in Figure 4. Diamonds and circles denote experiments in the towing tank (linear discharge) and tall tank (rotating discharge), respectively, while open and closed circles indicate crossflow- and stratification-dominated regimes of flow. Normalized particle sizes, U_s / U_c, are binned into four groups, each corresponding to a symbol size. The four groups of U_s / U_c, 0-0.3, 0.3-0.54, 0.54-1.01, and 1.01-1.96, are selected such that each group contains a similar number of experiments.

As illustrated in Figure 4, trap depth decreases with crossflow. This decreasing trend is consistent across both sets of experiments and both flow regimes, the transition between which depends on $U_{a,trans}$ [Equation (3)]. While the mechanisms of intrusion in a crossflow are complex (Dissanayake et al., 2018), the observed decrease is presumably due to the simple fact that crossflow enhances mixing of the plume with lighter ambient water near the discharge that in turn reduces the average density of the plume, making it trap closer to the discharge (smaller trap depth).

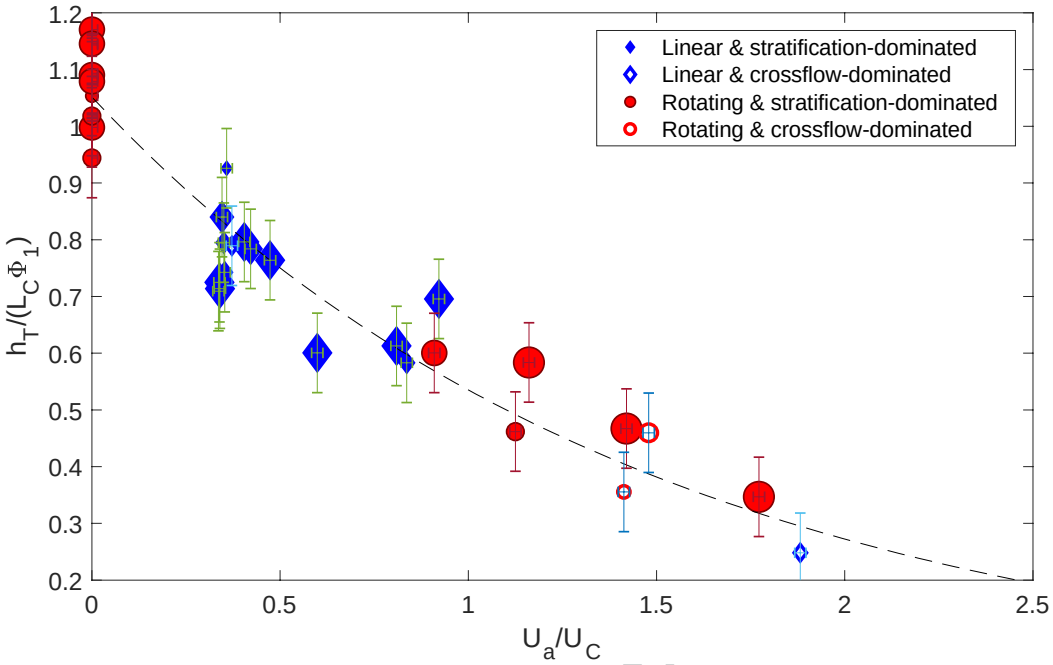

Figure 4. Observed plume trap depth reduces exponentially with increasing crossflow in laboratory experiments: (diamond) linear source and (circles) rotating source. Open and closed symbols indicate crossflow- and stratification-dominated regimes of flow, respectively. The non-dimensional particle sizes (U_s/U_c) are binned into four groups (0-0.3, 0.3-0.54, 0.54-1.01, and 1.01-1.96), with successively larger marker size as (U_s/U_c) increases. Trap depth shows little correlation with particle size, in the range studied. The error bars are computed as the averages of the standard deviations of repeat experiments. The average of the standard deviation in $h_T/L_c/\phi_1$ is 0.07 and in U_a/U_c it is 0.02.

The experimental results are best described by an exponential decay curve (black dashed line through the data points):

$$\frac{h_T}{L_c \emptyset_1} = \emptyset_2 \left[\frac{U_a}{U_C}\right] = e^{-0.60\frac{U_a}{U_C}}. \qquad (9)$$

Combining $\emptyset_1$ and $\emptyset_2$, the full expression for $\frac{h_T}{L_c}$ is given by:

$$\frac{h_T}{L_c} = (2.8 - 0.066\frac{U_s}{U_c})e^{-0.60\frac{U_a}{U_C}} . \qquad (10)$$

As shown in Figure 4, the model describes the average behavior of the laboratory measurement reasonably well. $\frac{h_T}{L_c}$ shows more dependence on ambient crossflow ($\emptyset_2$) than on particle settling velocity ($\emptyset_1$). In the limit of small particle size, and thus small settling velocity U_s, $\emptyset_1$ approaches a constant value of 2.8. In the limit of ambient velocity U_a approaching zero, $\emptyset_2$ approaches zero

and $\frac{h_T}{L_c}$ becomes dependent on $\emptyset_1$ only. In the limit of both small particle settling velocity and crossflow velocity, the model again approaches the value for a single phase plume where $\frac{h_T}{L_c} \approx 2.8$ (Morton et al., 1956).

4. Model application - PLUMEX field study

4.1. Introduction

Deep-sea mining of metals such as nickel, cobalt, copper and manganese is under consideration as a supplement to land-based mining operations; however, its environmental implications remain largely unknown. One particular environmental concern is the discharge of mining residuals (water and sediment brought up from the seafloor with the mined metals and then potentially released continuously in midwater as a sediment plume). To address the current knowledge gap, a field study, PLUMEX, was conducted to investigate aspects of the sediment plume including its trapping or intrusion behavior (Munoz-Royo et al., 2020).

The centerpiece of the study was PLUMEX5, a commercial-scale field experimental plume using a slurry comprised of seafloor sediment and ambient seawater that had been prepared in mixing tanks over the preceding several days aboard the research vessel. The sediment was originally collected from the Clarion-Clipperton Fracture Zone (CCFZ) in the Northeastern Pacific, with specific gravity of 2.6 and median grain size of 9-12μm. Consistent with Munoz-Royo et al., (2020), we assumed a constant settling velocity of 0.1mm/s, which is characteristic of a 10μm sediment particle. The PLUMEX5 slurry was released vertically downward through a flexible hose of inner radius of 10cm, at an average depth of 59m below the water surface continuously for 45 minutes, together with Rhodamine dye as a tracer.

The plume structure was monitored in the field using acoustic imaging (documenting the very near field plume within a few meters of the release), a custom microstructure profiler (documenting plume structure in the rebounding plume ~30 meters from the release), and a conductivity-temperature-depth instrument (CTD) with turbidity and fluorescence measurements (documenting the trapped plume ~ hundreds of meters from the release). Our focus here is the CTD measurements as these pertain to the trapped plume where the analytical model is applicable. The

field experimental conditions are summarized in Table 3. Additional details are provided in Munoz-Royo et al., (2020).

Table 3. Summary of PLUMEX5 (simulated sediment plume experiment) parameters at the discharge.

Dynamic plume parameters at discharge	CCFZ sediment plume
C_s: Initial sediment concentration(kg/m^3)	8 ± 1
ρ_a: Density anomaly (kg/m^3)	4.60 ± 0.2
V_e: Exit velocity (m/s)	1.46 ± 0.05
Q_0: Volume flux (m^3/s)	0.047 ± 0.002
M_0: Momentum flux (m^4/s^2)	0.069 ± 0.005
B_0: Buoyancy flux (m^4/s^3)	(2.10 ± 0.2) x 10^{-3}
Re: Reynolds number	(2.50 ± 0.1) x 10^5
Fr: Densimetric Froude number	22 ± 1
Discharge depth (m)	58.90 ± 0.30
Discharge duration (minutes)	45
N: average stratification frequency (s^{-1})	0.01
N_m: Momentum number	0.296
N_q: Volume number	3.15 x 10^{-3}

The computed momentum and volume numbers using Equations (5) and (6) are smaller than one for PLUMEX5, which is indicative of basically a buoyancy-driven flow.

The negatively buoyant PLUMEX5 plume overshot its level of neutral buoyancy, then returned to a quasi-steady trap depth, h_T a few tens of meters downstream from the release point. The value of h_T was determined from the field observed concentration profile of Rhodamine dye and turbidity, measured with fluorometers and a transmissometer attached to the CTD, which was 'tow-yo'ed' across the plume for about 6.3 hours. Figure 5 shows examples of fluorescence and turbidity

profiles taken at various times (locations), and from which the plume trap depth can be determined using signal processing approaches (see Supplementary Information, Section 2.1). A total of 121 downcast profiles were collected in the field and analyzed during this time, sampling a range of depths from 40 to 150m. As shown in Figure 5, most of the Rhodamine dye and turbidity profiles taken at the same time showed close resemblance to each other in terms of shape and peak location (average trap depth).

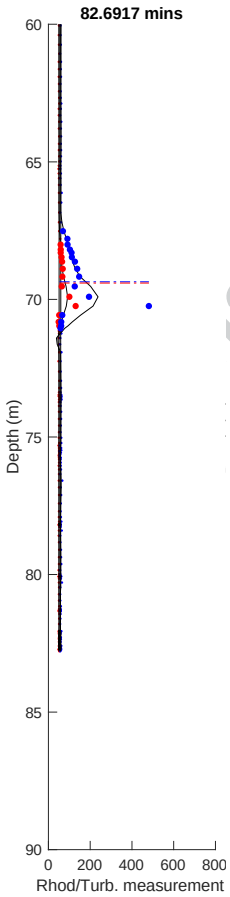

Figure 5. Sample downcast profile showing raw fluorescence (red dots) and turbidity (blue dots) measurement at each depth. Linear black lines are estimated background reading for each while the curved black lines represent best fit lines that are used to determine excess fluorescence and turbidity compared to the background. Bigger red and blue dots indicate measurements inside the plume and the red and blue broken horizontal lines are corresponding average plume depth computed based on these bigger dots. The profile was measured in the 83rd minute since the start of the plume release. This corresponds to a straight-line distance of about 500 m from the discharge (see Munoz-Royo et al., 2021 Section 2.3 and Figure 4 for more detail).

In addition to signal processing outlined in Supplementary Information Section 2.1, we corrected for the heaving (vertical motion) of the isopycnal surfaces (see Supplementary Information,

Section 2.3). The corrected h_T showed much less variation temporally (therefore spatially) within the first ~300 minutes (Figure 6 bottom; Supplementary Information, Section 2.2). This suggests the plume largely resided within the same isopycnal layer until ~300 minutes when the plume became slightly deeper (Figure 6 bottom). Analyzing the fluorescence and turbidity data for the field measurement period yielded a similar range of intrusion depth below water surface of between about 64m to 71m in the intermediate-field, and the same average of 66.3m for both types of measurements (Figure 6 bottom). Note that, for a discharge depth of 59m below the water surface, the average trap depth h_T would be 66.3 – 59 = 7.3 m. The range in depths could be attributed to the fluctuation in observed ambient velocity over the course of the measurement, to mixing with colder and saltier background ocean water from approximately 300 minutes to the end of the field measurement, and to the combination of vertical motion of the discharge pipe, caused by heaving of the ship on the ocean surface, and heaving of the ocean isopycnals (Munoz-Royo et al., 2020).

In Figure 6 top and bottom panels, the fact that turbidity and dye concentrations taken simultaneously matched well throughout the field measurement period suggests that minimal particle settling had occurred from the plume. This field observation is corroborated by estimating the settling depth as U_sT_s. Using a value of U_s = 0.1 mm/s, and T_s = 240 min (midway through the survey) (Munoz-Royo et al., 2020), yields an average settling depth of ~1.4 m, which is small compared with the plume thickness which was observed to be ~5 m as shown in the top panel of Figure 6. Certainly, there is a spectrum of sediment sizes, with some having more rapid settling velocity, but it seems clear that the dyed continuous phase of the plume had not completely "rebounded". Had field measurements been taken at longer elapsed times, the computed trap depth would have been slightly smaller.

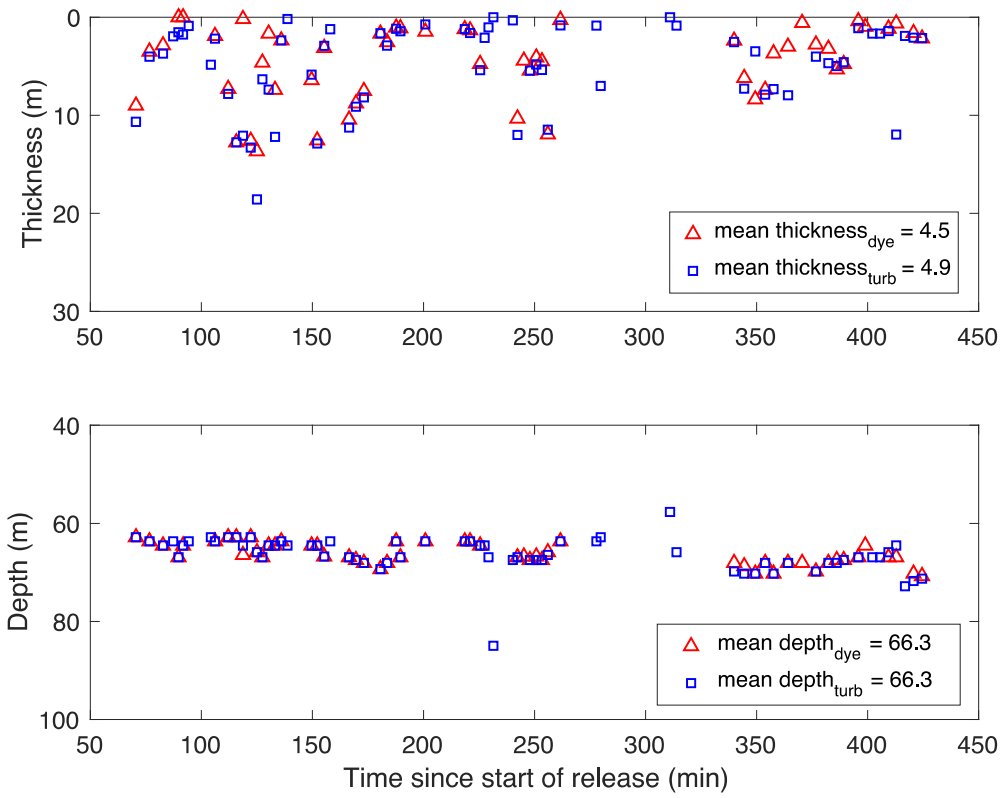

Figure 6. The measured intrusion thickness (top) and the intrusion depth (bottom) over time. In both panels, turbidity (open squares) and Rhodamine dye (open triangles) measurements are consistent with each other, suggesting little sedimentation of the fine particles. Measurements were taken over a period of approximately 7 hours and over a distance of about 2000 m. Note here the intrusion depth, h_T, is taken as the depth below sea surface whereas in the text h_T is referred to as depth below discharge level of 59m. We corrected for the effects of isopycnal variation on the h_T following procedure outlined in Supplementary Information, Section 2.3.

4.2. Analytical model prediction

The analytical model was used to predict the trap depth of the field release using measured parameter values from the field: a range of U_a between 7.3 cm/s and 13.9 cm/s and an average U_a of 10.6 cm/s based upon the ship's ADCP; an average N of 0.01 /s (values of N are computed using density profiles derived from CTD measurements); and B_0 of 0.0021 m^4/s^3. The resulting L_c and U_c are 6.77 m and 0.067 m/s, respectively. The range in observed trap depths is consistent with the range in analytical model predictions. The average observed value is slightly bigger than the predicted average (Figure 7). In dimensional terms, the difference between average observed and predicted trap depth is 0.1m.

4.3. Numerical model prediction for trap depth

To provide additional insight, a numerical model named TAMOC (Texas A&M Oil spill / Outfall Calculator) was used to simulate PLUMEX5. The model, developed by Texas A&M University, is a comprehensive numerical modeling suite that is capable of simulating both single- and multi-phase plumes in uniform or stratified fluid environments. (Dissanayake et al. 2018). TAMOC has two sub-models that consider the presence or absence of ambient crossflow current: The Stratified Plume Model (SPM) predicts the steady-state solution for plumes in quiescent environments; the Bent Plume Model (BPM) solves for the steady-state plumes in crossflow. While designed for positively buoyant bubbles or droplets, the model was adapted in this study to inert, negatively buoyant particles by matching their settling velocities. For details of the model and a list of the input parameters, see Dissanayake et al., (2018) and the present Supplementary Information Section 2.4, respectively.

4.3.1. Trap depth for multi-phase plume in weak crossflow

Firstly, we used TAMOC's Bent Plume Model to simulate the plume as a multi-phase flow. For the measured parameter values from the field, the corresponding range of trap depth simulated with TAMOC is given in Figure 7. Evidently, TAMOC overpredicts the trap depth, especially at low ambient velocities. This suggests that TAMOC may be less applicable to sediment plumes in weak crossflows for which the analytical model may be better suited. This may be due to the fact that the multiphase crossflow experiments used in the TAMOC calibration were all for bubble plumes and one buoyant oil droplet plume (Dissanayake et al. 2018). Bubbles have significantly different inertia than settling particle plumes, and these differences may not be captured in the model's current parameterization.

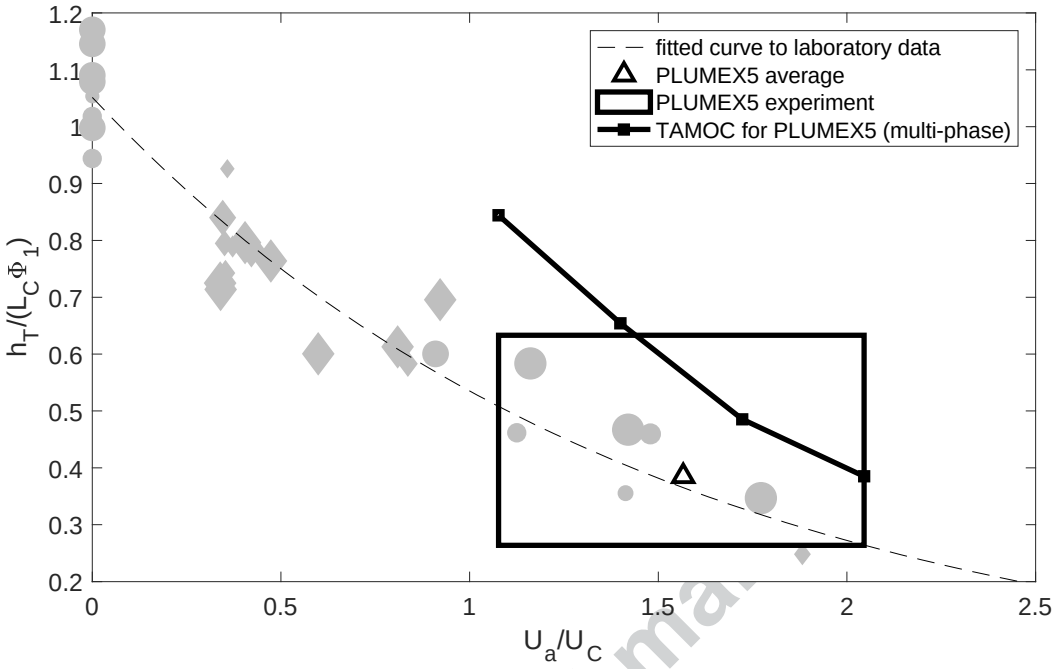

Figure 7. The normalized plume trap depth: (grey symbols) laboratory experimental data presented in Figure 4; (black box) PLUMEX5 field measurements; (black line) TAMOC simulations as a multi-phase plume; (open triangle) the average plume trap depth of PLUMEX5 corresponding to an average U_a of 10.6 m/s. The range of observed crossflow velocity resulted in the corresponding range of observed and simulated trap depths.

To further explore the TAMOC simulation of PLUMEX5, we simulated the plume as single-phase. This was done by computing an effective salinity, $S_{effective}$, for the plume that consisted of only the continuous phase (see Supplementary Information, Section 2.5).

The model results for the continuous-phase simulations in TAMOC show good agreement with the continuous-phase simulations presented in Figure 7, with at most a variation of 2.4% (simulated trap depth of the single-phase plume not shown in Figure 7). The close agreement is consistent with the slow settling velocity of the particles in the multi-phase plume.

5. Summary and Conclusions

The study presents two sets of laboratory experiments with different approaches to simulate crossflow velocity. The first set is conducted in a towing tank where the crossflow is simulated by towing the discharge linearly through a linearly stratified stagnant ambient. The second set is

carried out in a tall tank where the discharge is towed in a circular fashion through a linearly stratified stagnant ambient.

Plume trapping depths were observed and measured using *in-situ* fluorescence measurements. The trap depths decreased strongly with increasing crossflow velocity, suggesting that forced entrainment by the ambient current reduces the difference in density between the particle-fluid mixture and the receiving water, allowing the plume to reach a neutral buoyancy level sooner than in a slower crossflow. The fact that a single relationship holds for the entire set of laboratory measurements suggests that the role of force entrainment applies to both stratification- and crossflow-dominated plumes.

Based on measurements, an exponential equation was developed to relate normalized trap depth to normalized current speed. The simple model successfully fit the laboratory data and showed good agreement with larger scale field measurements -- a continuous sediment release resulting from deep sea mining operation.

6. Acknowledgement

Funding for this project was supported by the Center for Environmental Sensing and Modeling (CENSAM) laboratory in Singapore as part the Singapore-MIT Alliance for Science and Technology (SMART) Program, and by the BP/Gulf of Mexico Research Initiative, through the GISR consortium. The authors would like to thank Spencer Kawamoto, Mike Goldin, Jonathan Ladner, Sara Goheen and San Nguyen from the Scripps Multiscale Ocean Dynamics team, Captain Desjardins and the crew aboard the R/V Sally Ride, Global Sea Mineral resources (GSR) for supplying the CCFZ sediment and facilitating the cruise, the MIT Environmental Solutions Initiative. Any use of trade, firm, or product names is for descriptive purposes only and does not imply endorsement by the U.S. Government.

7. References

Akar, P. J., & Jirka, G. H. (1994). Buoyant spreading processes in pollutant transport and mixing Part 1: Lateral spreading with ambient current advection. *Journal of Hydraulic Research, 32*(6), 815–831. https://doi.org/10.1080/00221689409498692

Akar, P. J., & Jirka, G. H. (1995). Buoyant spreading processes in pollutant transport and mixing

Part 2: Upstream spreading in weak ambient current. *Journal of Hydraulic Research*, *33*(1), 87–100. https://doi.org/10.1080/00221689509498686

Asaeda, T., & Imberger, J. (1993). Structure of bubble plumes in linearly stratified environments. *J. Fluid Meeh*, *249*, 36–57. https://doi.org/10.1017/S0022112093001065

Chan, G. K. Y., Chow, A. C., & Adams, E. E. (2014). Effects of droplet size on intrusion of sub-surface oil spills. *Environmental Fluid Mechanics*, *15*(5), 959–973. https://doi.org/10.1007/s10652-014-9389-5

Chow, A. C. (2004). *Effects of buoyancy source composition on multiphase plume behavior in stratification*. MIT. Retrieved from http://hdl.handle.net/1721.1/16627

Dietrich, W. E. (1982). Settling velocity of natural particles. *Water Resources Research*, *18*(6), 1615–1626. https://doi.org/10.1029/WR018i006p01615

Dissanayake, A. L., Gros, J., & Socolofsky, S. A. (2018). Integral models for bubble, droplet, and multiphase plume dynamics in stratification and crossflow. *Environmental Fluid Mechanics*, *18*(5), 1167–1202. https://doi.org/10.1007/s10652-018-9591-y

Fischer, H., List, J., Koh, C., Imberger, J., & Brooks, N. (1979). *Mixing in Inland and Coastal Waters*. Elsevier. https://doi.org/10.1016/C2009-0-22051-4

Hill, D. F. (2002). General density gradients in general domains: The "two-tank" method revisited. *Experiments in Fluids*. https://doi.org/10.1007/s00348-001-0376-5

Johansen, Ø., Rye, H., & Cooper, C. (2003). DeepSpill-Field study of a simulated oil and gas blowout in deep water. *Spill Science and Technology Bulletin*, *8*(5–6), 433–443. https://doi.org/10.1016/S1353-2561(02)00123-8

Lemckert, C. J., & Imberger, J. (1993a). Axisymmetric Intrusive Gravity Currents in Linearly Stratified Fluids. *Journal of Hydraulic Engineering*, *119*(6), 662–679. https://doi.org/10.1061/(ASCE)0733-9429(1993)119:6(662)

Lemckert, C. J., & Imberger, J. (1993b). Energetic Bubble Plumes in Arbitrary Stratification. *Journal of Hydraulic Engineering*, *119*(6), 680–703. https://doi.org/10.1061/(ASCE)0733-9429(1993)119:6(680)

McDougall, T. J. (1978). Bubble plumes in stratified environments. *Journal of Fluid Mechanics*, *86*(4), 655–672. https://doi.org/10.1017/S0022112078000841

Mingotti, N., & Woods, A. W. (2019). Multiphase plumes in a stratified ambient. *Journal of Fluid Mechanics*, *869*, 292–312. https://doi.org/10.1017/jfm.2019.198

Morton, B. R., Taylor, G., & Turner, J. S. (1956). Turbulent Gravitational Convection from Maintained and Instantaneous Sources. *Proceedings of the Royal Society A: Mathematical, Physical and Engineering Sciences*, *234*(1196), 1–23. https://doi.org/10.1098/rspa.1956.0011

Munoz-Royo, C., Peacock, T., Alford, M. H., Smith, J., Boyer, A. Le, Kulkarni, C. S., … Se-Jong, J. (2020). Assessing the scale of deep-sea nodule mining midwater discharge sediment plumes. *Communications Earth & Environment. Under review*.

Socolofsky, S. A., & Adams, E. E. (2002). Multi-phase plumes in uniform and stratified crossflow. *Journal of Hydraulic Research*, *40*(6), 661–672. https://doi.org/10.1080/00221680209499913

Socolofsky, S. A., & Adams, E. E. (2005). Role of Slip Velocity in the Behavior of Stratified Multiphase Plumes. *Journal of Hydraulic Engineering*, *131*(4), 273–282. https://doi.org/10.1061/(ASCE)0733-9429(2005)131:4(273)

Wang, D., & Adams, E. E. (2016). Intrusion Dynamics of Particle plume in stratified water with weak crossflow : Application to deep ocean blowouts. *Journal of Geophysical Research: Oceans*, *121*, 1–16. https://doi.org/10.1002/2015JC011324

Wright, S. J. (1984). Buoyant Jets in Density-Stratified Crossflow. *Journal of Hydraulic Engineering*, *110*(5), 643–656. https://doi.org/10.1061/(ASCE)0733-9429(1984)110:5(643)